Model Predictive Control for Permanent Magnet Synchronous Motor Drives Considering Cross-Saturation Effects

Panagiotis Kakosimos*, Minos Beniakar† , Yushan Liu*, and Haitham Abu-Rub*

Email: {Panagiotis.Kakosimos, Yushan.Liu, Haitham.Abu-Rub}@qatar.tamu.edu Minos.Beniakar@se.abb.com

*Department of Electrical and Computer Engineering, Texas A&M University at Qatar, Education City, Doha, Qatar

†ABB AB, Corporate Research, Västerås, Sweden

***Abstract*—This paper presents a control strategy for permanent magnet synchronous motors (PMSMs) based on finite-state model predictive control (FS-MPC). The predictive model is enhanced by incorporating saturation and cross-coupling effects on the *dq*-axis flux linkages of the motor. Although a surface PMSM is used, the maximum torque per ampere (MTPA) trajectory is found dependent on both *dq*-axis currents and affected by geometrical saliencies. The dependence of the *dq*-axis inductances is inserted into the control law of the developed MPC routine, thus improving the model accuracy. The performance of the direct predictive torque controller is tested by controlling a PMSM drive supplied by a neutral-point clamped inverter. Implementation results have proven that the proposed control scheme can effectively satisfy the requirements that arise from both the PMSM and the inverter.**

Keywords—Permanent magnet drives, neutral-point clamped inverter, electric drive, nonlinear, predictive control.

I. Introduction

Nonlinear phenomena such as cross- or direct-coupling saturation effects are commonly found in interior PMSMs [1]. Although surface-mounted PMSMs do not contain a great deal of saliency, such phenomena appear when the motor is driven to the limits of current density [2], [3]. When the load or speed abruptly changes, the motor operates at maximum phase current directly saturating the stator and rotor laminations. In addition, the magnetic flux generated by the current of one axis is indirectly influenced by that of the other axis [4]. This interaction between the direct- and cross-coupling linkages necessitates the *dq*-axis inductances to be expressed as functions of both *dq*-axis currents.

Model predictive control (MPC), being capable of considering multi-variable control objectives, arises as a favorable option for the control of more complex and nonlinear systems [5]–[8]. By simultaneously satisfying control objectives that arise from both the motor and inverter, MPC provides an effective solution to electric drive applications. In literature, MPC has been successfully used to control topologies of increased complexity as well as high-performance drives [9]–[11]. However, the control requirements arising from an electric drive, which is fed by a more sophisticated inverter topology, are significantly more demanding [12]. The use of Multilevel Inverters (MIs), along with the consideration of nonlinearities, further increases the already increased system complexity [13]–[15].

Unlike linear control strategies, MPC enables the incorporation of nonlinear phenomena into the motor model [12], [16]. Embodying the direct- and cross-saturation effects into the motor equivalent circuit allows the controller to precisely control the motor over a wide range of loads and speeds [17]. In literature, there are several examples, where the performance of the drive was improved by the consideration of nonlinear effects. In [18], an approach was presented where the trajectory of the motor was extracted by unifying different dynamic trajectories. The developed controller offered accurate control of torque oscillations while improving the transient behavior of the drive. A continuous set nonlinear MPC strategy for PMSM drives was developed in [19]. The proposed method controlled the flux linkage of the motor allowing the consideration of nonlinear phenomena while keeping the switching frequency constant. In [20], a PMSM model was developed considering saturation induced saliencies. The derived model improved the performance of a sensorless control strategy minimizing the position dependent estimation errors.

In this paper, a predictive controller of an NPC inverter for PMSM drives is developed and presented. Saturation and cross-coupling effects on the motor *dq*-axis flux linkages are identified and incorporated into the predictive model improving its accuracy. In order to extract the parameters of the model and the MTPA trajectory, a systematized method is developed. The cross-coupling saturation of the *dq*-axis flux linkages and the existing geometrical saliencies considerably affect the MTPA trajectory even when surface-mounted PMSMs are used. The dependent parameters on the *dq*-axis currents are introduced into the predictive model and the control law of the MPC. The performance of the direct predictive torque controller has been evaluated by controlling a PMSM drive fed by an NPC inverter. Implementation results have proven that the requirements arising from both the PMSM and the inverter can be satisfied by the developed control scheme.

This publication was made possible by PDRA grant 2-1110-14066 from the Qatar National Research Fund (a member of the Qatar Foundation). The statements made herein are solely the responsibility of the authors.

II. PREDICTIVE MODEL

In high-performance motor drives, sophisticated control criteria are usually applied and the consideration of several control constraints is needed. The multivariable nature of MPC facilitates the implementation of control strategies with strict requirements. In this section, the complete drive system shown in Fig. 1 is described and the predictive model and the execution steps of MPC are given in more details.

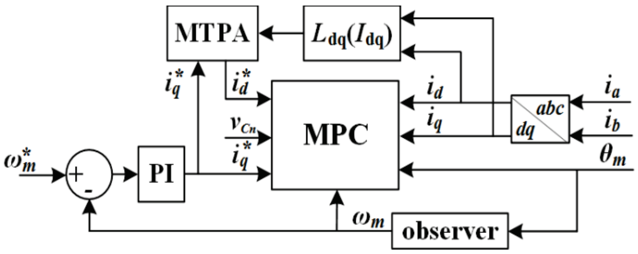

Fig. 1. Control strategy overview.

A. Plant modelling

The discrete electrical state-space model of the motor and inverter is used enabling MPC to predict the values of the controlled variables at the future sampling instants. Therefore, the system equations are expressed as function of the switching states of the inverter. MPC estimates the future behavior of the state variables by exploring all the available switching combinations. As shown in Fig. 2, the PMSM is fed by a three-level neutral-point clamped inverter. In order to avoid short-circuiting the DC bus, a switching rule governs each leg of the inverter. Only the two upper, middle and lower switches of each leg are allowed to be switched-on at the same time. The parameter, T, is used in order to express the three output voltage levels as function of the switching states as next:

$$T_{x=a,b,c} = [1,0,-1] \rightarrow v_{xo} = \left[v_{C1}, 0, -v_{C2}\right], \tag{1}$$

$$\begin{aligned} T_x &= \;\;\,1 \rightarrow S_{1x} = S_{2x} = 1 \\ T_x &= \;\;\,0 \rightarrow S_{2x} = S_{3x} = 1 \\ T_x &= -1 \rightarrow S_{3x} = S_{4x} = 1 \end{aligned} \tag{2}$$

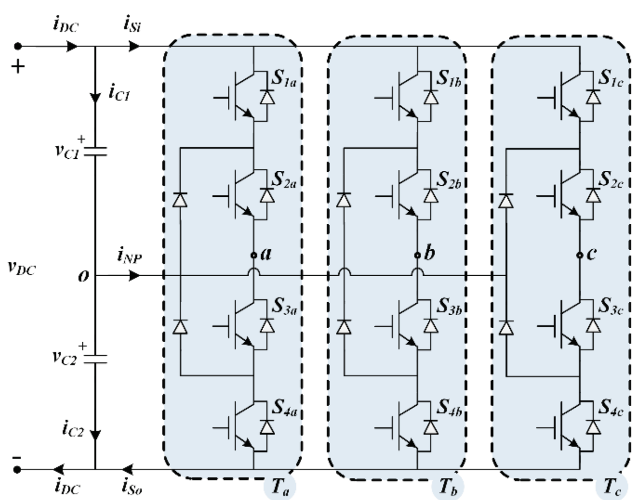

Fig. 2. Neutral-point clamped inverter.

The total switching combinations of the inverter are 27 (= 3^3), 8 of which are redundant. The stator voltages of the PMSM can be calculated in the dq-reference frame by using:

$$v_d = Ri_d + \frac{d\lambda_d}{dt} - \omega\lambda_q\,, \tag{3}$$

$$v_q = Ri_q + \frac{d\lambda_q}{dt} + \omega\lambda_d\,, \tag{4}$$

where R is the stator resistance, ω is the electrical speed and λ is the total flux linkage of the dq axes. More specifically, the flux linkage of the q-axis is $\lambda_q = L_q i_q$, whereas the flux linkage of the d-axis is $\lambda_d = L_d i_d + \lambda'_m$. L_d and L_q are the dq-axis inductances and λ'_m is the flux linkage of the permanent magnets. The d-axis flux linkage also includes the flux produced by the permanent magnets (PMs). The flux of the PMs is mainly affected by temperature conditions or extensive operation in the field-weakening region and it is not significantly dependent on the dq-axis currents. On the other hand, the inductances are dependent on the currents of both axes. Therefore, the derivatives of the time-variant terms of (3)-(4) can be calculated as follows:

$$\frac{d\lambda_q}{dt} = \frac{d}{dt}\underbrace{\left[L_q(i_d,i_q)i_q\right]}_{\lambda_q}, \tag{5}$$

$$\frac{d\lambda_d}{dt} = \frac{d}{dt}\underbrace{\left[L_d(i_d,i_q)i_d + \lambda'_m\right]}_{\lambda_d}. \tag{6}$$

Since the sampling time of MPC is significantly small, the dq-axis inductances and the flux linkage of the permanent magnets are considered constant and time independent. The values of the dq-axis inductances can now be incorporated into the control law of MPC. For the convenience of programming, the derived state-space model of PMSMs is discretized and expressed in matrix form as follows:

$$\hat{x}_{k+1} = \mathbf{A}x_k + \mathbf{B}u_k + \mathbf{E}\,, \tag{7}$$

$$\hat{y}_{k+1} = \mathbf{C}\hat{x}_{k+1}\,, \tag{8}$$

where the state vector is $x = \left[i_d, i_q\right]^T$. The notation (^) is used hereafter for the estimated values. By using the mathematical model of PMSMs and applying Euler discretization method, the system matrices used in (7)-(8) are calculated:

$$\mathbf{A} = \begin{bmatrix} 1 - \dfrac{RT_s}{L_d(i_d,i_q)} & \dfrac{L_q(i_d,i_q)T_s}{L_d(i_d,i_q)}\omega \\ -\dfrac{L_d T_s}{L_q(i_d,i_q)}\omega & 1 - \dfrac{RT_s}{L_q(i_d,i_q)} \end{bmatrix}, \quad \mathbf{C} = \begin{bmatrix} 1 & 0 \\ 0 & 1 \end{bmatrix}, \tag{9}$$

$$\mathbf{B} = \begin{bmatrix} \dfrac{T_s}{L_d(i_d,i_q)} & 0 \\ 0 & \dfrac{T_s}{L_q(i_d,i_q)} \end{bmatrix}, \quad \mathbf{E} = \begin{bmatrix} 0 \\ -\dfrac{\lambda T_s}{L_q(i_d,i_q)}\omega \end{bmatrix}, \tag{10}$$

where T_s is the discretization time. The output vector, y, is identical with the state vector, x, because the state and controlled variables are the dq-axis motor currents. In order to associate the switching states with the predicted values of the controlled variables, the control vector, $u = [u_d, u_q]^T$, is used. The following conversion matrices **M** and **D** are needed to transform the control vector from the three-phase representation system into the dq-reference frame.

$$\mathbf{M} = \begin{bmatrix} \sin\theta & -\cos\theta \\ \cos\theta & \sin\theta \end{bmatrix}, \tag{11}$$

$$\mathbf{D} = \frac{v_{DC}}{3} \begin{bmatrix} 1 & -\frac{1}{2} & -\frac{1}{2} \\ 0 & \frac{\sqrt{3}}{2} & -\frac{\sqrt{3}}{2} \end{bmatrix}, \tag{12}$$

where θ is the electrical angle at the sampling instant k. The electromagnetic torque can be estimated at the end of the prediction stage of the motor currents as follows:

$$\hat{T}_{e,k+1} = \frac{3}{2} p \left(\underbrace{\left(\lambda'_m + L_d \hat{i}_{d,k+1}\right)}_{\lambda_d} \hat{i}_{q,k+1} - \underbrace{L_q \hat{i}_{q,k+1}}_{\lambda_q} \hat{i}_{d,k+1} \right), \tag{13}$$

where p is the number of pole pairs. In (12), it has been assumed that the potential of the neutral point is indeed kept at zero level; thus, the total voltage of the DC-link has been used in the calculations instead of the voltage of each capacitor. This assumption allows significant simplification of the calculations and decreases the control variables. Regarding this assumption, the neutral-point balance has to be ensured under any operating condition; otherwise, the controller operation will be unsuccessful.

B. Neutral-point potential balance

In order for the controller to keep the DC-bus capacitors well-balanced, the time for which each inverter leg dwells on the middle point, o, needs to be adjusted. If the voltage across the capacitors' terminals is unbalanced, the total harmonic distortion of the output voltage is directly affected. Furthermore, the stress of the semiconductors is increased and the power losses are unevenly distributed [9], [21]. MPC can regulate the voltage difference by expressing the voltages of the capacitors as function of the switching combinations. In literature, there are several methods ensuring that the voltage difference is kept at zero level [22]. Most methods require the sensing of the capacitor currents and the DC input current in order to predict the unbalance level at the next sampling period [23]. In this study, a different approach is followed without demanding the measurement of both currents [10]. The potential of the neutral point is predicted instead of the capacitors' voltages. This approach allows the minimization of the necessary transducers.

More specifically, the current flowing to the common point of the clamping diodes can be estimated by using the phase currents and the condition of the switches as follows:

$$\hat{i}_{NP,k+1} = (T_c^2 - T_a^2) i_{a,k} + (T_c^2 - T_b^2) i_{b,k}, \tag{14}$$

where $i_{x,k+1} \approx i_{x,k}$ because the variation of the motor current is significantly slower. The neutral-point current is equal to the difference between the currents of the DC-link capacitors. By using the following discrete-time differential equation, the neutral-point potential can be predicted:

$$\Delta\hat{v}_{NP,k+2} = \Delta v_{NP,k+1} + \frac{T_s}{C} \hat{i}_{NP,k+1}, \tag{15}$$

where the voltage unbalance is estimated for two sampling periods ahead demanding the controller to compensate for this delay and to correct the initialization in the prediction process.

C. Cost function

Using the developed model, the controller can estimate the value of the state variables at the end of the next N sampling instants by evaluating all the switching combinations. The combination that minimizes the cost function is selected and applied by the controller. The adopted cost function has the following form:

$$J_k = \sum_{i=1}^{N} \left(C_{T,k+i} + C_{id,k+i} + R_{NP,k+i} + R_{im,k+i} \right). \tag{16}$$

In (16) there are two different types of errors, the tracking, C, and the restriction, R, errors. The first errors involve the tracking of the torque and the d-axis current, whereas the restriction errors involve the neutral-point balance and the maximum phase current:

$$C = \underbrace{w_T (\hat{T} - T^*)^2}_{C_T} + \underbrace{w_{id} (\hat{i}_d - i_d^*)^2}_{C_{id}}, \tag{17}$$

$$R = \underbrace{w_{NP} \Delta\hat{v}_C^{\,2}}_{R_{NP}} + \underbrace{w_{im} \left(\sqrt{\hat{i}_q^2 + \hat{i}_d^2} - \mathrm{I_m} \right)^2}_{R_{im}}. \tag{18}$$

The quadratic errors are multiplied by the corresponding weighting factors, w. Since the controlled variables are expressed in different units, the main goal of the weights is to normalize these errors.

D. Execution steps

At a first step, the analogue-to-digital (A/D) converters of the digital controller sample the state variables and convert them to digital. Given the fact that the process of A/D acquisition and the examination of the possible switching states require significant time to be completed, there is a delay between the calculations and the actual change of the switching state. The actual values of the sensed state variables are corrected by considering the control output of the previous sampling period as follows:

$$\tilde{x}_k = \mathbf{A} x_k + \mathbf{B} u_{k|k-1} + \mathbf{E}. \tag{19}$$

At the next step of the control algorithm, the potential of the neutral-point, the state variables and the torque are estimated and the cost function is evaluated for all the possible switching states.

Algorithm: *Execution of the MPC algorithm*

System initialization (J_{min} = inf, ind = 1)
Sensing of ω_m, $i_{x|x=a,b}$ and v_{Cn}
Delay compensation
for n = 1, 2, ..., 27
    Estimation of $\hat{\imath}_{dq,k+1}$, $\widehat{\Delta v}_{NP,k+1}$ and $\hat{T}_k$
    Selection of the weighting factors
    $J_{k+1} = C_{T,k+1} + C_{id,k+1} + R_{im,k+1} + R_{NP,k+1}$
    if $J_{k+1} < J_{min}$ **then** $J_{min} = J_{k+1}$ and $ind = n$ **end if**
  end for
end for

Fig. 3. Execution steps of MPC.

III. Nonlinear Parameter Extraction

For the extraction of the dq-axis inductances, Finite-Element Analysis (FEA) is used. The distribution of the flux density of the used PMSM is shown in Fig. 4. Due to the nonsymmetrical winding configuration, the flux density distribution is significantly affected suggesting that the conventional motor model is not suitable for the prediction of the state variables. The magnetic fluxes generated by the dq-axis currents saturate some parts of the stator and rotor laminations and the flux lines of the one axis cross those of the other axis affecting the inductances of the motor.

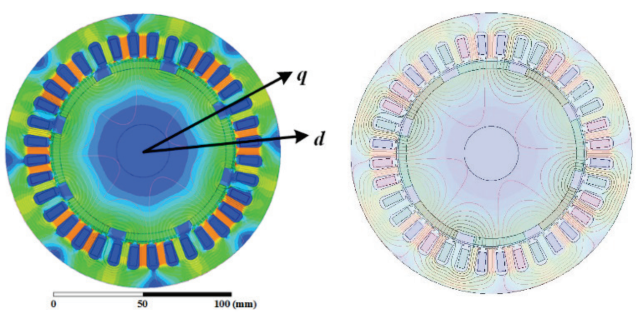

Fig. 4. Flux density of the PMSM.

Algorithm: *Parameter extraction*

Initialize rotor and stator position
for i_s = 0:0.4:6
    T_{max} = 0
    for θ_e = 0:15:180
        for t = 0:1/6 of period
            Calculate the dq-axis flux linkages and torque
        end for
        if $T > T_{max}$ **then** store θ_e **end if**
  end for
end for

Fig. 5. Parameter extraction methodology.

For extracting the parameters of the model and determining the MTPA trajectory, the algorithm described in Fig. 5 has been developed. Firstly, the relevant position of the rotor and stator is initialized aligning the d-axis with the axis of phase a. Afterwards, the amplitude and the angle of the phase current are increased to the maximum permissible values. The torque is calculated and the current vector of the maximum produced torque is stored defining the MTPA curve. In order to increase the accuracy of the calculations, transient analysis is performed considering the one-sixth of the electrical period and averaging the values of the calculated parameters. Afterwards, the extracted parameters are incorporated into the control law of MPC. In the main routine of MPC, the dq-axis inductances and the MTPA trajectory are calculated with respect to the dq-axis currents [10].

IV. Results and Discussion

In this section, the extracted fluxes of both axes are presented and the developed MPC strategy is evaluated by exploring several test-case scenarios. The main characteristics of the motor, the inverter and the predictive controller are summarized in Table I.

Table I. System Specifications

Parameter	*Value*	*Parameter*	*Value*
Pole pairs	4	D-axis inductance	18 mH
DC-link voltage	400 V	Sampling time	100 us
DC-bus capacitors	3 mF	*Weights*	
PM flux linkage	1 Wb	Torque,w_T	0.05
Winding resistance	6 Ω	D-axis current,w_{id}	0.25
Nominal current	3 A	NP potential,w_{NP}	0.10
Moment of inertia	0.02 kgm^2	Max. current,w_{im}	10^6

A. Cross-saturation effects

By applying the parameter extraction methodology of the previous section, the dq-axis fluxes shown in Fig. 6 and Fig. 7 have been found. The d-axis flux shown in Fig. 6, is the total flux of the d-axis including the flux linkage of the magnets as described in (6). Both fluxes are not absolutely symmetric about the dq axes, due to the asymmetry between the number of stator slots and pole pairs of the examined motor topology. Although a surface-mounted PMSM is used, it is shown that as the q-axis current increases, the d-axis flux linkage decreases. On the other hand, when the d-axis current increases, the q-axis flux decreases.

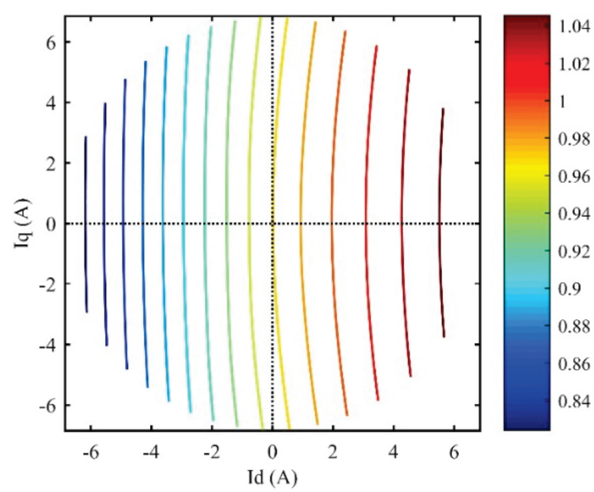

Fig. 6. D-axis flux linkage (in Wb).

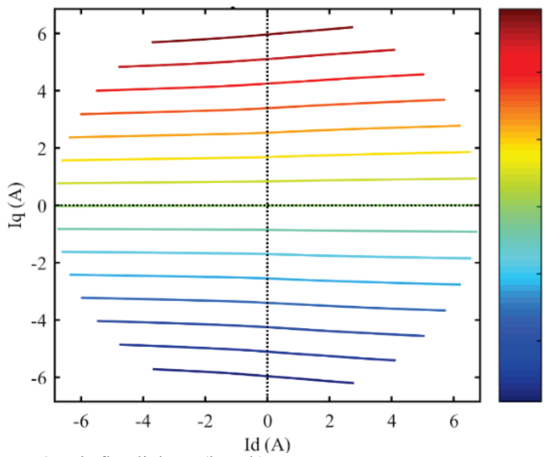

Fig. 7. Q-axis flux linkage (in Wb).

Despite that the coupling between the dq-axis inductances and currents is not strong, the negligence of the cross-saturation is expected to negatively affect the performance of the drive system. In addition, an accurate motor model is also essential in the operation of several control strategies, such as in sensorless control strategies as reported in [20]. Furthermore, the derived fluxes can be fine-tuned by conducting extensive experiments.

B. Predictive controller

After using the parameter extraction algorithm, the dq-axis flux linkages are expressed as functions of the dq-axis currents and inserted into the control scheme of MPC. The performance of the developed MPC is evaluated in this section by exploring several test-case scenarios. The developed MPC is implemented into a dSpace controller requiring 100µs sampling time for the algorithm execution. The adopted prediction and control horizon is one step ahead. Firstly, the drive system has been tested performing speed reversal (from -40 to +40 rad/s) at nominal load conditions. As shown in Fig. 8, the developed MPC precisely tracks the speed reference, while the phase current is kept below the maximum permissible value.

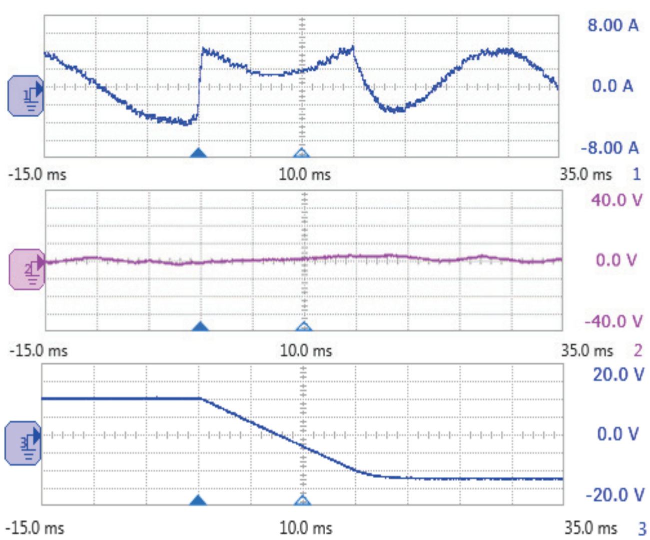

Fig. 8. Speed reversal.
1. Phase current. 2. Neutral-point potential. 3. Speed (4 rad/Vs).

In order to investigate the effectiveness of the incorporation of the cross-saturation effects, the controller has been also tested keeping constant the motor reference speed at 40 rad/s and changing the torque profile of the load as shown in Fig. 9. More specifically, at t = 0 s, the load torque changes from 40 Nm to zero and then changes direction to -40 Nm. During the change of the load torque profile, the neutral-point potential is kept at zero level. On the other hand, the motor speed is not considerably affected when the load torque changes. In Fig. 10, the calculated MTPA curve and the actual trajectory of the motor are shown. It is important to highlight, that although a surface-mounted PMSM is used, the MTPA trajectory is not aligned with the q-axis ($i_d = 0$).

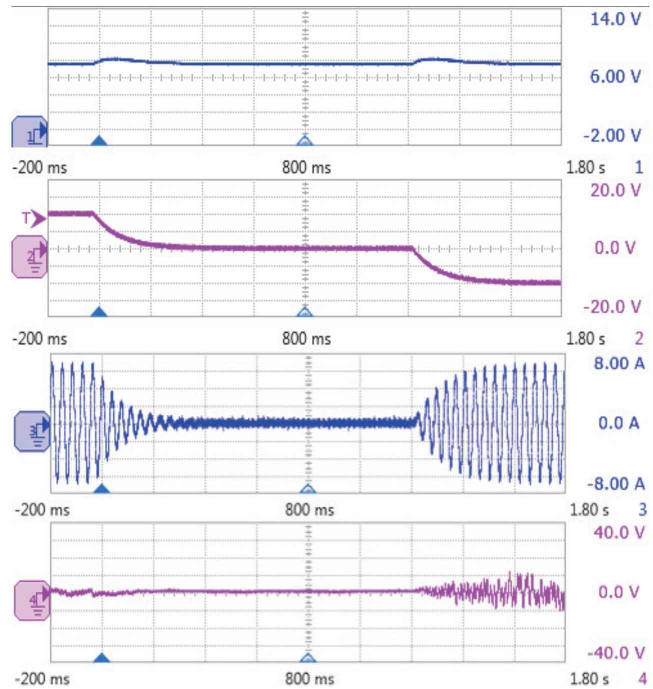

Fig. 9. Load profile change.
1. Speed (6 rad/Vs). 2. Load torque profile (4 Nm/V).
3. Phase current. 4. Neutral-point potential.

During the operation shown in Fig. 9, the motor accurately tracked the MTPA trajectory. Due to the cross-saturation effects, the d-axis inductance decreased by 4.52%, whereas the q-axis inductance by 4.03%. The torque-per-ampere ratio was found 6.05 Nm/A_p, increased by 3.2% compared to the operation without considering the cross-coupling effects. The improvement is expected to be higher as the current density increases. For higher current density, the trajectory is expected to deviate from the q-axis due to the presence of stronger cross-coupling and saturation effects. Operation under high current is common in several applications such as in aerospace, where the actuator has to operate at extreme conditions for several minutes [3]. At high speeds, the coupling of the dq-axis inductances is also expected to be higher, negatively affecting the performance of the motor.

V. Conlusion

This paper presented a predictive torque controller of an NPC inverter for PMSM drives. The accuracy of the predictive model was improved by incorporating direct- and cross-saturation effects on the motor parameters. The dependent parameters on the *dq*-axis currents were inserted into the predictive model and the control law of the developed MPC. Although a surface-mounted PMSM was used, the MTPA trajectory was affected by the cross coupling of the *dq*-axis flux linkages and the geometrical saliencies of the motor. Implementation results proved that the suggested control strategy increased the torque-per-ampere ratio and accurately tracked the MTPA trajectory.

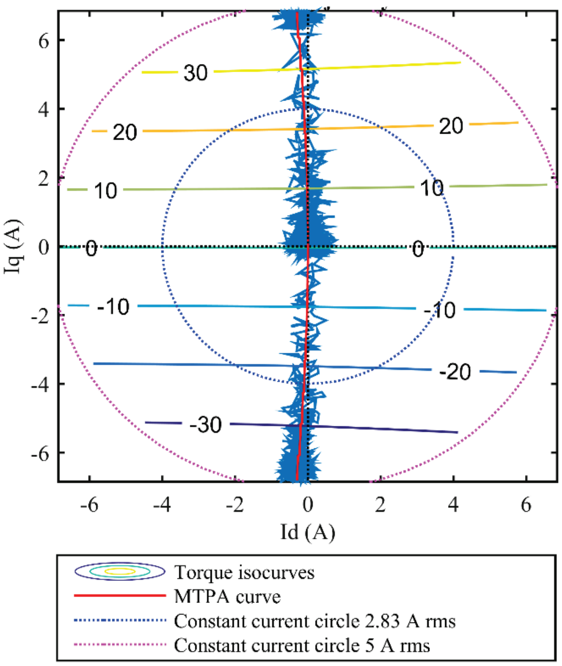

Fig. 10. MTPA trajectory for the operation shown in Fig. 9.

References

[1] Y. Wang, J. Zhu, and Y. Guo, “A Comprehensive Analytical Mathematic Model for Permanent-Magnet Synchronous Machines Incorporating Structural and Saturation Saliencies,” *IEEE Trans. Magn.*, vol. 46, no. 12, pp. 4081–4091, Dec. 2010.

[2] M. Seilmeier and B. Piepenbreier, “Modeling of PMSM with multiple saliencies using a stator-oriented magnetic circuit approach,” in *International Electric Machines & Drives Conference*, 2011, pp. 131–136.

[3] P. Kakosimos, A. Sarigiannidis, M. E. Beniakar, A. Kladas, and C. Gerada, “Induction Motors Versus Permanent-Magnet Actuators for Aerospace Applications,” *IEEE Trans. Ind. Electron.*, vol. 61, no. 8, pp. 4315–4325, Aug. 2014.

[4] P. Kakosimos and A. Kladas, “Modeling of interior permanent magnet machine using combined field-circuit analysis,” in *19th IEEE International Conference on Electrical Machines*, 2010, pp. 1–6.

[5] M. Preindl and S. Bolognani, “Model Predictive Direct Torque Control With Finite Control Set for PMSM Drive Systems, Part 1: Maximum Torque Per Ampere Operation,” *IEEE Trans. Ind. Informatics*, vol. 9, no. 4, pp. 1912–1921, Nov. 2013.

[6] T. Geyer, G. Papafotiou, and M. Morari, “Hybrid Model Predictive Control of the Step-Down DC–DC Converter,” *IEEE Trans. Control Syst. Technol.*, vol. 16, no. 6, pp. 1112–1124, Nov. 2008.

[7] E. Fuentes, D. Kalise, J. Rodriguez, and R. M. Kennel, “Cascade-Free Predictive Speed Control for Electrical Drives,” *IEEE Trans. Ind. Electron.*, vol. 61, no. 5, pp. 2176–2184, May 2014.

[8] P. Kakosimos, A. Kladas, and S. Manias, “Fast Photovoltaic-System Voltage- or Current-Oriented MPPT Employing a Predictive Digital Current-Controlled Converter,” *IEEE Trans. Ind. Electron.*, vol. 60, no. 12, pp. 5673–5685, Dec. 2013.

[9] J. D. Barros, J. F. A. Silva, and E. G. A. Jesus, “Fast-Predictive Optimal Control of NPC Multilevel Converters,” *IEEE Trans. Ind. Electron.*, vol. 60, no. 2, pp. 619–627, Feb. 2013.

[10] V. Yaramasu, M. Rivera, M. Narimani, B. Wu, and J. Rodriguez, “High performance operation for a four-leg NPC inverter with two-sample-ahead predictive control strategy,” *Electr. Power Syst. Res.*, vol. 123, pp. 31–39, Jun. 2015.

[11] H. Abu-Rub, A. Iqbal, and J. Guzinski, *High Performance Control of AC Drives with MATLAB/Simulink Models*. Chichester, UK: John Wiley & Sons, Ltd, 2012.

[12] J. Rodriguez, R. M. Kennel, J. R. Espinoza, M. Trincado, C. A. Silva, and C. A. Rojas, “High-Performance Control Strategies for Electrical Drives: An Experimental Assessment,” *IEEE Trans. Ind. Electron.*, vol. 59, no. 2, pp. 812–820, Feb. 2012.

[13] K.-H. Kim, “Model reference adaptive control-based adaptive current control scheme of a PM synchronous motor with an improved servo performance,” *IET Electr. Power Appl.*, vol. 3, no. 1, p. 8, 2009.

[14] H. Abu-Rub, J. Holtz, J. Rodriguez, and G. Baoming, “Medium-Voltage Multilevel Converters: State of the Art, Challenges, and Requirements in Industrial Applications,” *IEEE Trans. Ind. Electron.*, vol. 57, no. 8, pp. 2581–2596, Aug. 2010.

[15] P. Kakosimos, S. Bayhan, and H. Abu-Rub, “Single-phase Cascaded H-bridge Neutral-Point Clamped Inverter: A comparison between MPC and PI control,” in *42nd Annual Conference of IEEE Industrial Electronics Society*, 2016.

[16] M. Preindl and S. Bolognani, “Model Predictive Direct Torque Control With Finite Control Set for PMSM Drive Systems, Part 2: Field Weakening Operation,” *IEEE Trans. Ind. Informatics*, vol. 9, no. 2, pp. 648–657, May 2013.

[17] Z. Q. Zhu, Y. Li, D. Howe, C. M. Bingham, and D. Stone, “Influence of Machine Topology and Cross-Coupling Magnetic Saturation on Rotor Position Estimation Accuracy in Extended Back-EMF Based Sensorless PM Brushless AC Drives,” in *IEEE Industry Applications Annual Meeting*, 2007, pp. 2378–2385.

[18] J. Richter and M. Doppelbauer, “Predictive Trajectory Control of Permanent-Magnet Synchronous Machines With Nonlinear Magnetics,” *IEEE Trans. Ind. Electron.*, vol. 63, no. 6, pp. 3915–3924, Jun. 2016.

[19] Z. Ma and S. S. R. Kennel, “Continuous set nonlinear model predictive control for PMSM drives,” in *15th European Conference on Power Electronics and Applications*, 2013, pp. 1–10.

[20] M. Seilmeier, S. Ebersberger, and B. Piepenbreier, “PMSM model for sensorless control considering saturation induced secondary saliencies,” in *International Symposium on Sensorless Control for Electrical Drives and Predictive Control of Electrical Drives and Power Electronics*, 2013, pp. 1–8.

[21] P. Kakosimos, K. Pavlou, A. Kladas, and S. Manias, “A single-phase nine-level inverter for renewable energy systems employing model predictive control,” *Energy Convers. Manag.*, vol. 89, pp. 427–437, Jan. 2015.

[22] J. Rodriguez, S. Kouro, M. Rivera, M. Narimani, B. Wu, and V. Yaramasu, “Generalised approach for predictive control with common-mode voltage mitigation in multilevel diode-clamped converters,” *IET Power Electron.*, vol. 8, no. 8, pp. 1440–1450, Aug. 2015.

[23] R. Vargas, P. Cortes, U. Ammann, J. Rodriguez, and J. Pontt, “Predictive Control of a Three-Phase Neutral-Point-Clamped Inverter,” *IEEE Trans. Ind. Electron.*, vol. 54, no. 5, pp. 2697–2705, Oct. 2007.